Optical-vortex pair creation and annihilation and helical astigmatism of a nonplanar ring resonator

N. R. Heckenberg,* M. Vaupel, J. T. Malos,* and C. O. Weiss
Physikalisch-Technische Bundesanstalt, 38116 Braunschweig, Germany
(Received 1 December 1995)

The creation and annihilation of pairs of optical vortices have been studied in transitions between patterns produced in a photorefractive oscillator. Smooth metamorphosis between stable patterns occurs through pair creation or annihilation but can be modeled using superposition of modes taking into account lifting of degeneracy of helical modes by helical astigmatism of the resonator. [S1050-2947(96)04508-8]

PACS number(s): 42.55.−f, 42.65.Hw

I. INTRODUCTION

It has been previously demonstrated that lasers and photorefractive oscillators (PRO's) can emit fields with vortices that remain intact as they move along circular paths about the optic axis [1]. The patterns containing the vortices can be understood as simultaneous emission of helical fields with high topological charge phase singularities together with rotationally symmetric fields such as the fundamental Gaussian mode. The number and distribution of vortices and the vortex charges consequently depend upon which modes are contributing to the total field pattern. The frequency difference between modes gives rise to the dynamics of the patterns [1].

We report here experiments on the transient dynamics that occur when the cavity of a PRO is tuned between patterns containing different numbers and charges of vortices. In Sec. II, we present patterns for two resonator tuning positions; a pattern with four circling vortices and a pattern with five oppositely circling vortices of the same topological charge with one additional oppositely charged vortex in the center. The total topological charge of both patterns is the same whereas the total number of vortices differs by two so that a ''vortex pair'' has been created during the transition between the patterns.

In Sec. III, the number of vortices observed in the patterns, their arrangement, topological charge, and also circling direction are quantitatively simulated using a superposition of passive cavity helical modes. Here the modes and their respective amplitudes are chosen empirically. The dynamics are produced by introducing time-varying phase factors between the modes, which corresponds to the frequency differences between modes.

In Sec. IV, the details of the vortex pair creation are shown for situations where the tuning is changing (Sec. IV A) and when the tuning is fixed and the phase of the field varies (Sec. IV B). Furthermore, the detailed way in which a pair of oppositely charged vortices is created or annihilated is evident from the dynamics of the zero lines of the real and imaginary parts of the field. This is again determined from the passive cavity mode superposition for fixed amplitudes of the cavity modes corresponding to fixed tuning.

The pattern with 5 vortices circling a central vortex of opposite topological charge is obtained by a superposition of charge minus 1 and charge plus 4 doughnut modes. However, since the helical modes plus 4 and minus 4 should be frequency degenerate, a pattern corresponding to a superposition of plus 1 and plus 4 ought to be equally observable. Since this was never observed, we conjecture that the plus and minus charged helical modes of the same charge strength are frequency nondegenerate.

We show, in Sec. V, the principle of removing the frequency degeneracy of oppositely charged helical modes of the same charge strength by the use of a nonplanar ring cavity. This is experimentally verified by observation of the change in sign of a charge 1 doughnut mode with tuning of the cavity.

The setup is essentially the same as that of [1]. A unidirectional ring resonator of perimeter 2 m is used with an even number of mirrors to allow emission of fields with vortices. The resonator consists of 4 plane mirrors (2 of which are movable by piezo), polarizing beam splitters (used for active cavity length stabilization), a BSO crystal as the active photorefractive medium, two lenses to define the mode structure and select the number of transverse modes per free spectral range, and an iris to control the losses of the modes. The resonator length is actively stabilized with one piezo and transverse mode selection is achieved by moving the mirror with the second piezo. The lenses are placed such that the transverse mode spacing is slightly more than a quarter of the free spectral range. The transverse mode-selecting piezo is manually controlled. The tuning can be changed between desired positions on a time scale roughly comparable to the characteristic circling time of the vortices. Thus the tuning is quasistatic and not transient. For optical amplification in the resonator the BSO crystal is pumped by an Ar^+, 514 nm single-mode laser whose irradiance is around 3 mW/cm^2. An electric field is applied to the crystal (10–11 kV/cm) since BSO is a drift-type photorefractive material. Finally, 5% of the generated field is coupled out and recorded by a charge-coupled device camera.

II. EXPERIMENTALLY OBSERVED PATTERNS

Figures 1(a) and 1(b) show single frames of circling vortex patterns obtained from the output of the PRO for two

*Permanent address: Physics Department, The University of Queensland, Brisbane, Australia.

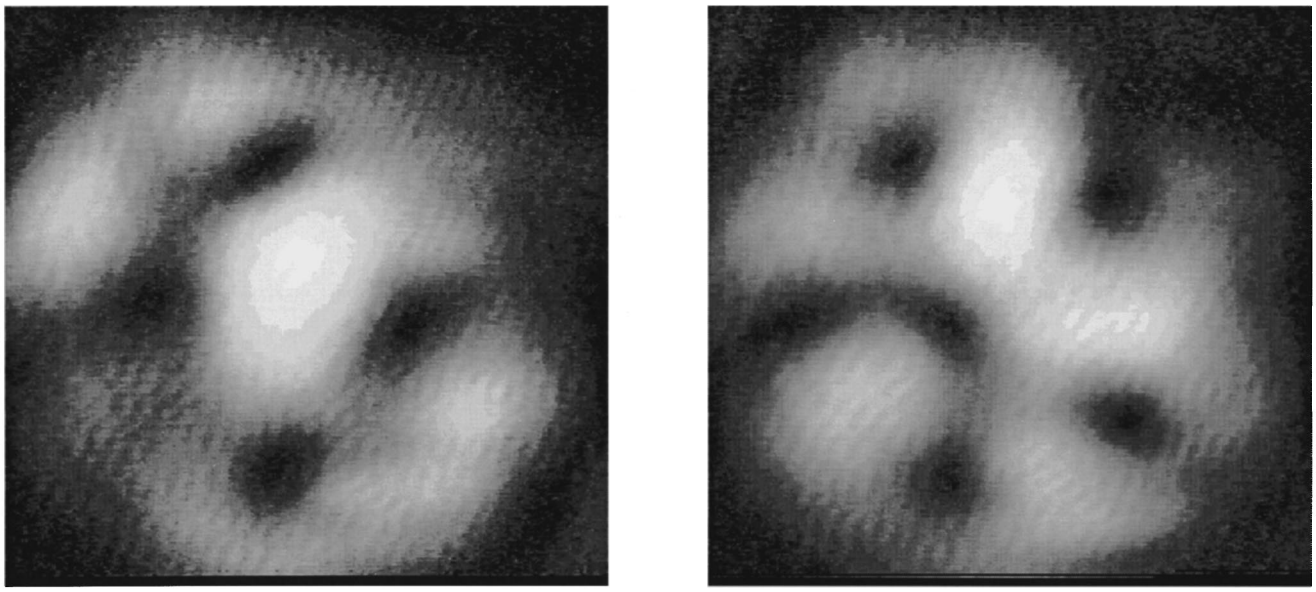

FIG. 1. Output patterns from the PRO for two different cavity tunings: Pattern (a) shows the presence of 4 optical vortices, which circle anticlockwise as viewed, and pattern (b) shows 5 vortices circling a 6th central vortex clockwise.

separate tuning positions of the cavity. The direction of circling is opposite between patterns (a) and (b).

Shown in Fig. 2 are the corresponding interferograms. It can be seen that in Fig. 2(a) there are four vortices of the same topological charge and in Fig. 2(b) there are five vortices of the same charge as in Fig. 2(a) with an additional vortex of opposite charge in the center. During the transition from pattern (a) to (b), therefore, a vortex pair appears. Locally about each vortex, the phase of the optical field changes by 2π but the phase change in the field around a vortex pair is zero. Thus the addition of a vortex pair does not change the total topological charge of the optical field.

The two cavity tuning positions for the above patterns are represented diagrammatically in Fig. 3 where the response of the cavity is shown as a function of frequency. Theoretically, each mode exhibits a Lorentzian response with a width and height dependent upon its losses, which we assume are higher for higher order modes. Direct measurements of such a curve were given in [1] and we have also verified that the ''active'' modes observed when the device is oscillating cor-

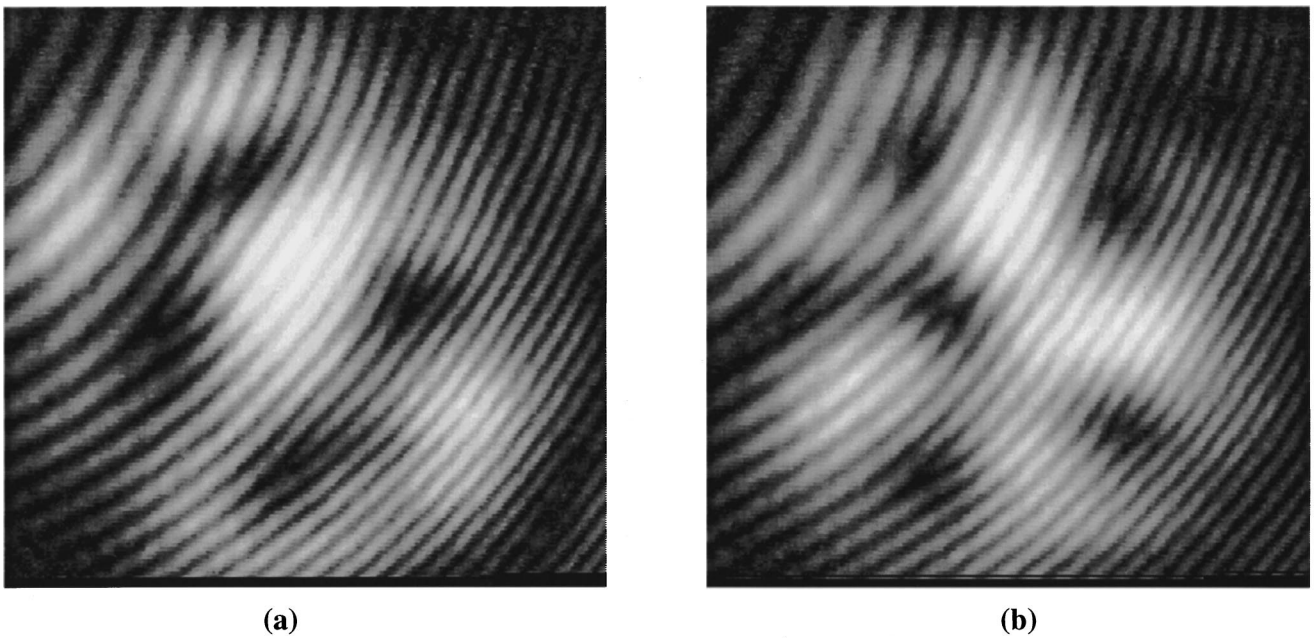

FIG. 2. Interferograms of Fig. 1 showing topological charge of vortices. The 4 vortices in pattern (a) all have the same topological charge as demonstrated by the interference fringe ''forks'' all pointing ''up.'' These are of the same charge as the 5 circling vortices in (b) and the 6th central vortex is oppositely charged.

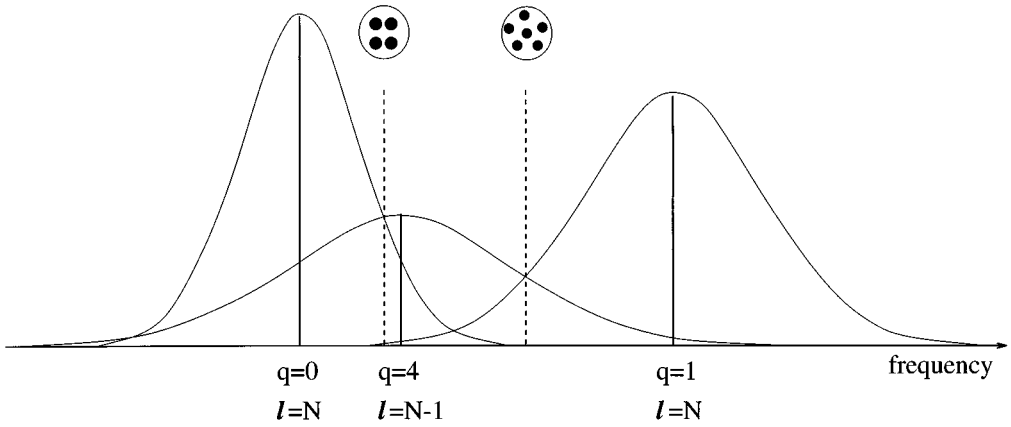

FIG. 3. Relationship between cavity modes and circling vortex patterns. The transmission of transverse modes of the passive cavity as a function of frequency is shown schematically. The frequency difference between TEM_{00} and TEM_{01} is about 40 MHz. The $q=4$ mode family from the $l=N-1$ longitudinal mode falls between that of the $q=0$ mode and the $q=1$ mode family for the $l=N$ longitudinal mode but is closer to the $q=0$ mode. The dotted lines represent the two cavity tuning positions corresponding to the patterns of Fig. 1.

respond directly with those observed in such a ''passive'' measurement (see also [2]).

The number of transverse modes per free spectral range for the cavity configuration producing the patterns in Fig. 1 is slightly less than 4. This means that the $q=4$ mode family from the $l=N-1$ longitudinal mode has a frequency between that of the $q=0$ mode and the $q=1$ mode family for the $l=N$ longitudinal mode, but close to the $q=0$ mode. The pattern of four circling vortices was experimentally obtained at a tuning between the $q=4$ charge 4 helical mode and the $q=0$ mode but close to the $q=4$ mode, as indicated in Fig. 3. The pattern is therefore the result of simultaneous emission of these two mode fields. The patterns of five circling vortices of ''like'' charge with a central vortex of opposite charge was obtained at a tuning position between the $q=4$ mode and the $q=1$ mode, but toward the $q=1$ mode so that the $q=0$ Gaussian mode is no longer significant. During the tuning, the $q=4$ mode continues to emit while the emission of the $q=0$ mode is replaced by $q=1$ emission.

In both (a) and (b) the vortices circle the optic axis. However, the direction of circling is opposite between (a) and (b). If two cavity modes have a constant difference in frequency, then the relative phase difference between the modes will constantly increase or decrease, depending upon which mode is chosen as the reference. It can then be understood that since the $q=4$ mode family frequency is higher than the $q=0$ mode and lower than the $q=1$ mode family, the phase differences, relative to the $q=4$ mode family, will correspondingly decrease and increase respectively with time. For a helical mode, a phase shift corresponds to a rotation. This gives rise to the circling dynamics and accounts for the change in circling direction observed between the two patterns, as will be demonstrated in the next section. Because of the extremely narrow gain linewidth of the PRO, massive frequency pulling occurs [3,4], reducing the rotation frequencies to values in the sub-Hertz range but maintaining the ratios of mode amplitudes [5].

III. PASSIVE CAVITY HELICAL MODE ANALYSIS

The transverse electric field amplitude in an optical cavity is described here as a simple superposition of the passive cavity mode functions using polar coordinates:

$$\psi(\rho,\varphi,t)=\sum_{q,l} C_{q,l}e^{i\Delta\omega_{q,l}t}A_{q,l}(\rho,\varphi). \tag{1}$$

Here $A_{q,l}$ are the Gauss-Laguerre modes chosen to represent the observed field and $C_{q,l}$ are their respective amplitudes. $\Delta\omega_{q,l}$ is the frequency difference between the (q,l) mode and some chosen reference mode (here the $A_{0,0}$ mode) so that the exponential term describes the time varying phases between the modes. $|\psi|^2$ is proportional to the intensity. The Gauss-Laguerre modes have the form

$$A_{q,l}(\rho,\varphi)=\left(\frac{2q!}{\pi(q+|l|)!}\right)^{1/2}(\sqrt{2}\rho)^{|l|}L_q^{|l|}(2\rho)e^{il\varphi}e^{-\rho^2}, \tag{2}$$

where

$$L_q^{|l|}(\rho)=\sum_{m=0}^{N}(-1)^m\binom{N+|l|}{N-m}\frac{\rho^m}{m!}. \tag{3}$$

Given the situation illustrated in Fig. 3, the modes chosen are the Gaussian mode, $A_{0,0}$, and the plus-minus charge 1 and 4 helical modes, $A_{0,\pm1}$ and $A_{0,\pm4}$, respectively:

$$\begin{aligned} A_{0,0}(\rho,\varphi)&=A_0=\sqrt{2/\pi}e^{-\rho^2},\\ A_{0,\pm1}(\rho,\varphi)&=A_1^{\pm}=\sqrt{1/\pi}2\rho e^{\pm i\varphi}e^{-\rho^2},\\ A_{0,\pm4}(\rho,\varphi)&=A_4^{\pm}=\sqrt{1/12\pi}4\rho^4e^{\pm4i\varphi}e^{-\rho^2}. \end{aligned} \tag{4}$$

Figure 4 shows the calculated transverse intensity patterns for the following superpositions:

$$\begin{aligned} \psi_a&=A_0+e^{i\Delta\omega_4 t}A_4^{+},\\ \psi_b&=e^{i\Delta\omega_1 t}A_1^{-}+e^{i\Delta\omega_4 t}A_4^{+}, \end{aligned} \tag{5}$$

where $|\psi_a|^2$ and $|\psi_b|^2$ correspond to the intensity of the patterns in Figs. 4(a) and 4(b). $\Delta\omega_4$ and $\Delta\omega_1$ are the difference

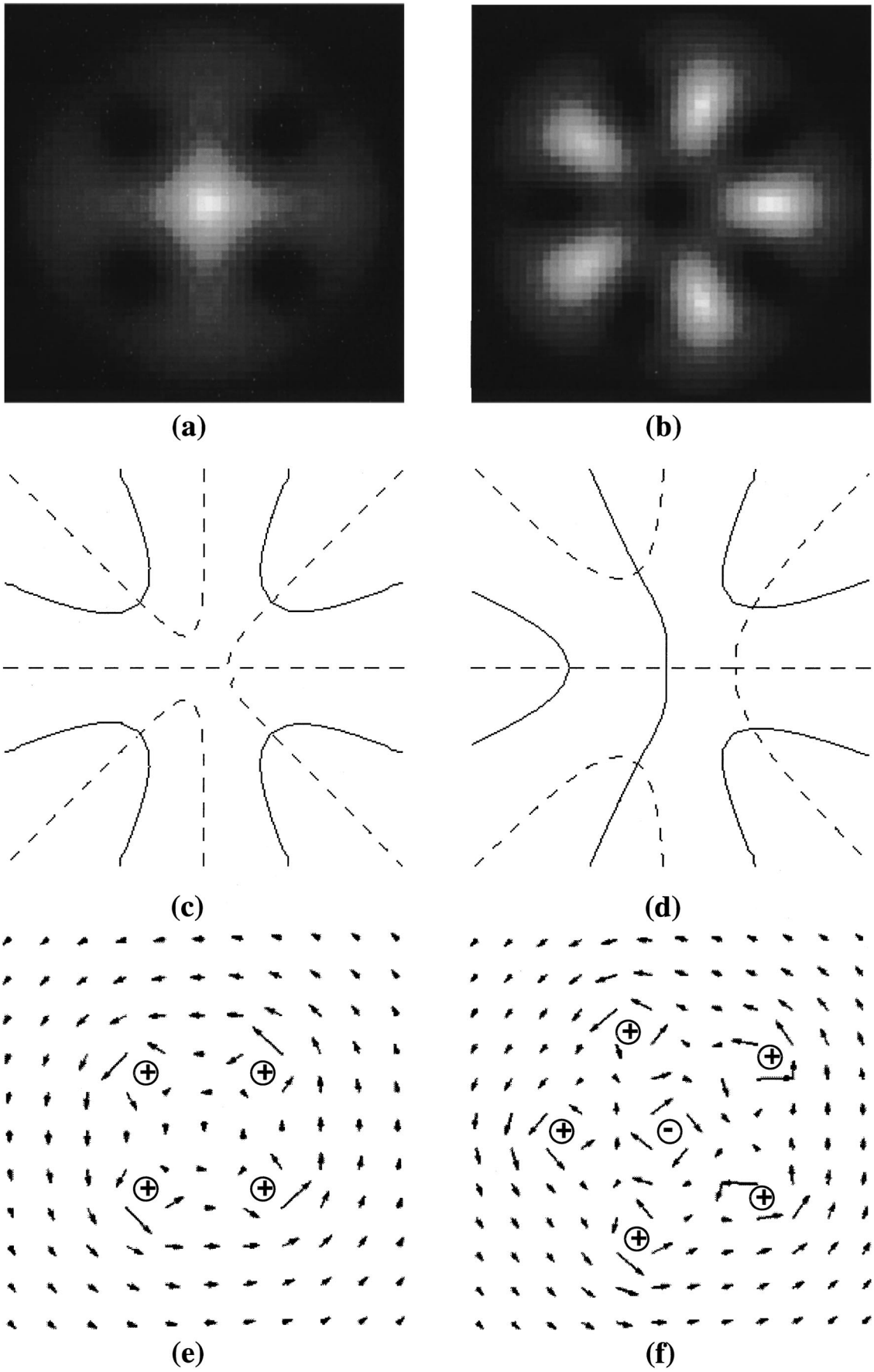

FIG. 4. (a) Calculated intensity patterns for the superposition of A_0 and A_4^+. (b) Superposition of A_1^- and A_4^+. (c),(d) Real (solid) and imaginary (dotted) zeros of the field corresponding to (a) and (b), respectively. The position where a real and an imaginary zero line cross indicates a zero in the field. (e),(f) The transverse component of the gradient of phase of the field corresponding to (a) and (b), respectively, demonstrating the presence of a vortex at the zero points of the field. (e) has 4 anticlockwise vortices and (f) has 5 anticlockwise vortices circling a central clockwise vortex.

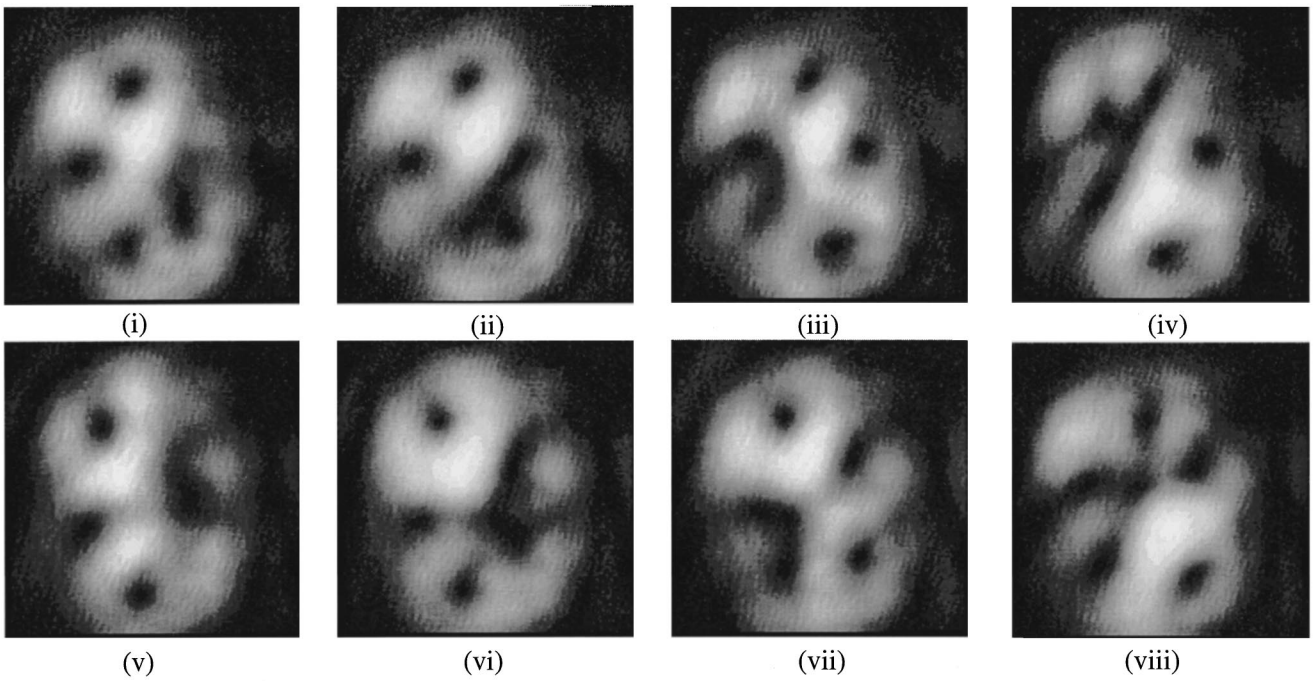

FIG. 5. Sequence of frames (selected from a continuous recording) showing the evolution of the pattern of Fig. 1(a) to that of 1(b). The piezo voltage has been changed so as to tune the cavity between the positions indicated by the two dotted lines in Fig. 3 over a period of 2 s.

frequencies between the $q=4$ and $q=0$ modes and between the $q=1$ and $q=0$ modes, respectively, where the $q=0$ mode is chosen as the reference frequency. We have $\Delta\omega_1>\Delta\omega_4>0$ so as to correspond to the situation of Fig. 3, where the frequency of the $q=4$ mode family lies between the $q=0$ mode and the $q=1$ mode family. The superposition of (5) gives the correct intensity distribution of the vortices corresponding to the observed patterns of Fig. 1. The patterns also rotate about the origin in opposite directions when the phases, $\Delta\omega_4 t$ and $\Delta\omega_1 t$, change with the time, in agreement with the experimental observations. Figures 4(c) and 4(d) show the zero lines of the real and imaginary parts of the field, $\mathrm{Re}\{\psi\}$ and $\mathrm{Im}\{\psi\}$. Vortices are found at the zero points in the field, where the real and imaginary loci intersect. Thus in Fig. 4(c) there are four zeros and in 4(d) there are six. To demonstrate the vortex nature of the zeros of the field and also to show the sign of the topological charge of the vortices, the gradient of the phase function of the field, $\nabla\Phi$, is plotted in Figs. 4(e) and 4(f) (the phase function is defined by $\psi=Ce^{i\Phi(\rho,\varphi,t)}$ [6]). The direction of circulation of the optical phase gives the sign of the topological charge of the vortex, as marked in the figures. It can been seen that (e) contains 4 anticlockwise vortices and (f) has 5 anticlockwise vortices arranged around the central clockwise vortex. These figures are in agreement with the experimental observations in Fig. 2.

Of course, the actual direction of phase circulation and hence ''charge'' or ''handedness'' of the vortices cannot be seen in the interferograms of Fig. 2. What can be directly observed is that the pattern of Fig. 2(a) has 4 vortices with interference fringe ''forks'' pointing ''up'' and are hence all of a particular charge. Figure 2(b) has 5 vortices of the same charge as in (a) and 1 of opposite charge. The choice of the A_4^+ and A_0^- modes in the superposition of Eq. (5) assumes that the ''up'' interference fringe ''forks'' correspond to positive topological charge and anticlockwise circulation of the optical phase. If the converse charge superposition is chosen (A_4^- and A_0^+ modes) then the only difference is that the ''up'' interference fringe ''forks'' would correspond to negative charge and clockwise circulation of the optical phase. The qualitative agreement to the experimental observations is unaffected.

In each of the cases studied, we have been able to match the observed patterns and their dynamics by simple superpositions of modes. Although we are not able to independently predict the amplitudes of the modes in the experiment as they depend upon unknown loss and gain distributions, the amplitudes chosen are plausible in the circumstances. In fact a hyperbolic tangent function (see Fig. 6 and 7) was used to generate smooth increases and decreases of the mode amplitudes in the instances where tuning between modes occurs and the mode amplitudes consequently vary. This empirical model leads to approximately correct values for the radii at which the singularities circles, which is sufficient for the current qualitative analysis.

IV. VORTEX-PAIR CREATION

The sequence of frames in Fig. 5 shows the transition from the pattern of Fig. 1(a) to 1(b). The creation of a vortex pair can be observed, for example, in Fig. 5(ii) where three vortices can be separated into a single vortex and a vortex pair. We have presented the detail of this pair creation in two ways. Firstly, the resonator tuning is varied between the dotted lines of Fig. 3 so that the mode amplitudes vary. However, frames are taken in a stroboscopic manner where the phase of the pattern is the same. That is, the location of the

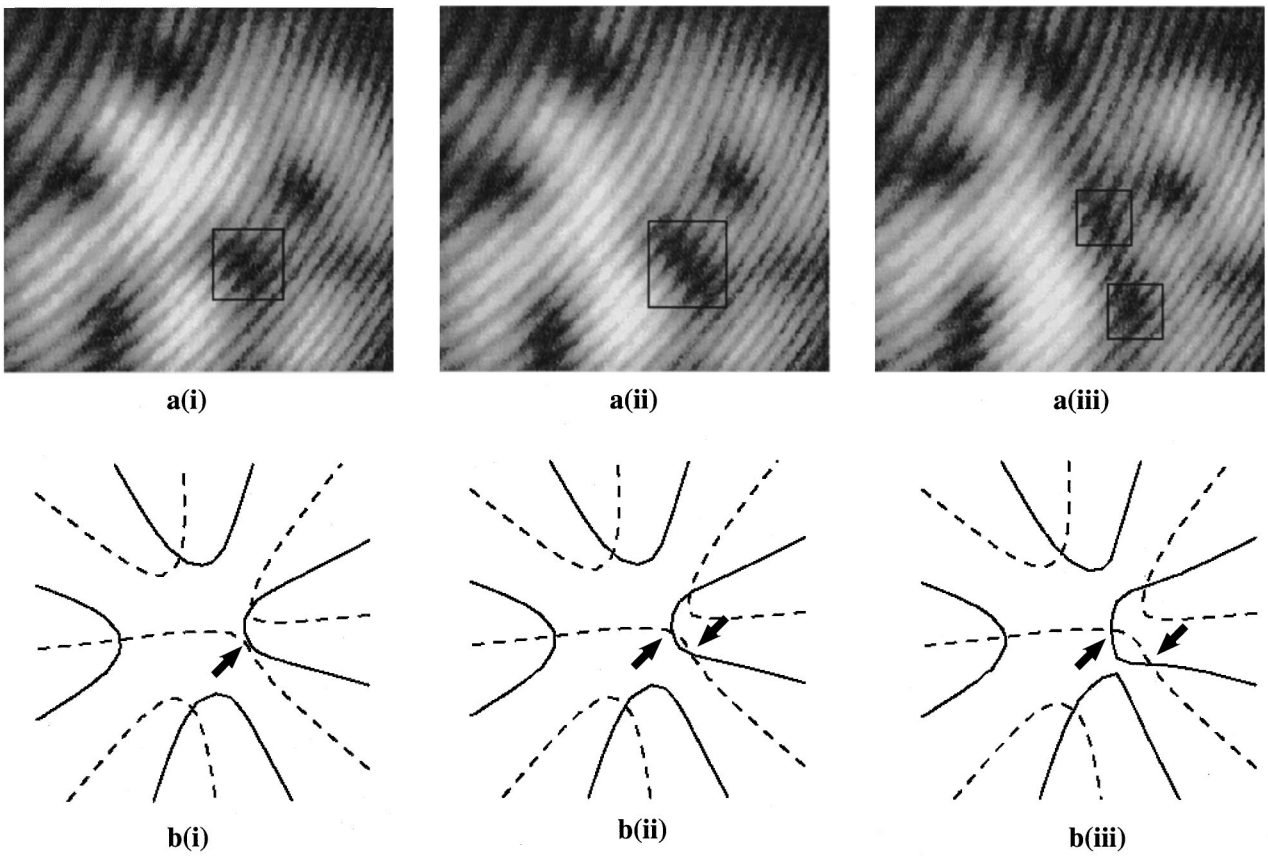

FIG. 6. Sequence of experimental frames (a) and the calculated real and imaginary zero loci (b) detailing vortex-pair creation with varying tuning observed at a chosen phase of the field. These frames are taken when the dark area, where vortex-pair creation takes place, is at the same angular position. The time between frames is roughly half a second. (a)(i) There are four dislocations present in the interference pattern corresponding to four zero points in the field where vortices are present. There is a fifth dark spot (indicated) but no dislocation. (a)(ii) After the tuning is changed, a vortex pair is now present as two opposite ''forks'' in the interference pattern. (a)(iii) The vortex pair is now clearly separated into two vortices of opposite topological charge. (b)(i) The vortex pair is close to being created where the real and imaginary loci are close together (indicated by the arrow). This is observed as a dark region in the field. (b)(ii) The real and imaginary loci have evolved so that they now intersect to form two extra vortices. (b)(iii) The intersection points are now clearly distinct. The real and imaginary loci are calculated from Eq. (6) using mode amplitudes, C_0, C_1, C_4, given by $C_0 = 1 - \tanh[\pi(j/N - 1/2)]$, $C_1 = 1 + \tanh[\pi(j/N - 1/2)]$, $C_4 = 1$, where $N = 40$ and $j = 21,\ 23,\ 26$, (b)(i), (b)(ii), and (b)(iii), respectively.

vortex-pair creation (annihilation) rotates around to the same position between the stroboscopically sampled frames. Secondly, the resonator is fixed at some tuning value somewhere between the dotted lines so that the mode amplitudes remain constant. In this case the periodic creation and annihilation of a vortex pair can be followed as the relative phase differences between the modes evolve.

A. Stroboscopic frames with varying tuning

Figure 6 shows the experimental interferograms (a) and the real and imaginary zero loci of the field (b). The dark spot marked by the rectangle in Fig. 6 rotates once around the center of the pattern between each of the frames (a)(i), (a)(ii), and (a)(iii). These frames are taken when the dark area, where vortex-pair creation takes place, is at the same angular position. However, the amplitude ratios between constituent modes, $C_0/C_1/C_4$, are changed as a result of resonator tuning. In terms of mode superposition this can be represented using the mode functions already defined as

$$\psi = C_0 A_0 + C_1 e^{i\Delta\omega_1 t} A_1^- + C_4 e^{i\Delta\omega_4 t} A_4^+ . \qquad (6)$$

Since we have $\Delta\omega_4 < \Delta\omega_1$, and given that the circling dynamics of the outer vortices is related to $\Delta\omega_4$, [1] the outer vortices do not move very much during 2π phase change of $\Delta\omega_1 t$. This is evident in Figs. 6(a)(i)–6(a)(iii). For this reason, in the calculation we can neglect $\Delta\omega_4 t$ and the motion of the dark area can be determined by $\Delta\omega_1 t$. Hence the condition $\Delta\omega_1 t = \varphi_0 + 2\pi n$ ($\varphi_0 = \text{const}$, n integer) corresponds to the dark area being in the same angular position between different strobe frames, $n = 0,\ 1,\ 2$ for Figs. 6(a)(i)–6(a)(iii).

In the experiment, the time for tuning between desired tuning positions is roughly comparable to the characteristic circling time of the vortices. Thus as the tuning is varied, the relative proportions of the modes simultaneously present will be in quasiequilibrium with the cavity tuning position. Of course, a dynamical analysis of the current system would provide a more accurate and representative determination of the variation of the mode amplitudes and indeed, the description of the cavity modes themselves. However, since the PRO is operated close to threshold, the system behaves as a class-A laser [7] and, as will be subsequently demonstrated,

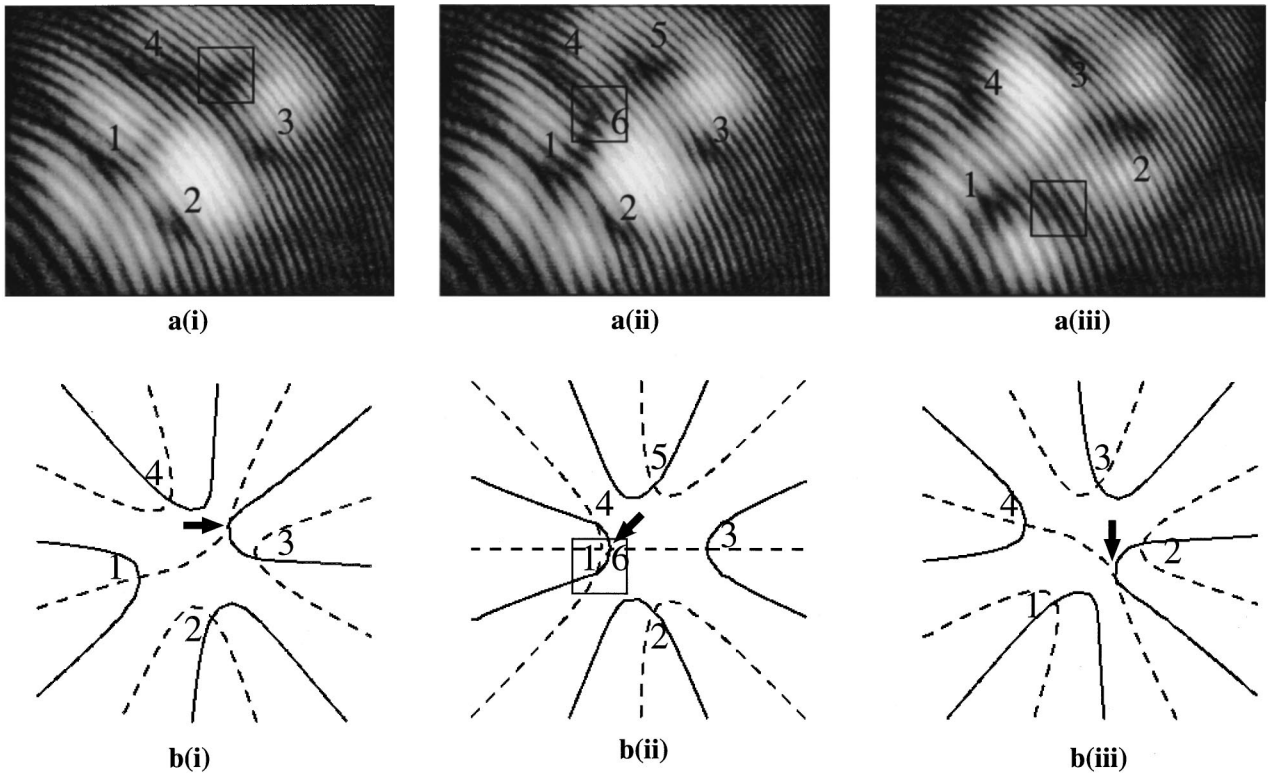

FIG. 7. Sequence of experimental frames (a) and the real and imaginary zero loci (b) detailing vortex-pair creation with a fixed cavity tuning: (a)(i) As in Fig. 6 a fifth dark spot is present but has no dislocation. (a)(ii) After the phase has evolved a small amount, a vortex pair is now present, with the innermost vortex being of opposite charge to the outer circling vortices. (a)(iii) Further evolution of the phase shows that the inner vortex has annihilated with one of the outer vortices and the vortex pair no longer exists. This whole process occurs over a time scale of about one-quarter to one-half second. (b)(i) The vortex pair is close to being created where the real and imaginary loci are close together. (b)(ii) The real and imaginary loci have evolved so that they now intersect to form two extra vortices. (b)(iii) The loci no longer intersect and the vortex pair is annihilated. The real and imaginary loci are calculated from Eq. (6) using the specific values given by $\psi = 0.35A_0 + 0.65e^{i8\pi j/N}A_1^- + e^{i4\pi j/N}A_4^+$, where $N=20$ and $j=3,\ 5,\ 7$ for (b)(i), (b)(ii), and (b)(iii), respectively.

the qualitative agreement between the observed patterns and those predicted from a passive cavity mode description is very good. The patterns can be well described without inclusion of such factors as cavity loss, gain saturation, and the effect of frequency pulling, which are not considered here.

The point at which the vortex pair is created can be seen from these figures. In Fig. 6(a)(i), there is a fifth dark spot in the field (indicated by the box) where there is no dislocation present and hence no vortex. In the corresponding diagram showing the real and imaginary zero loci, 6(b)(i), the dark spot corresponds to the position where the loci are closely spaced. In Fig. 6(a)(ii), the dark spot now has two oppositely directed dislocation forks demonstrating the presence of a vortex pair. This corresponds to the situation in Fig. 6(b)(ii) where the real and imaginary zero loci cross and vortices are found at the intersection points, as indicated. By further tuning, the vortex pair is now clearly separated so that there are five like-charge vortices arranged around the central oppositely charged vortex. Hence the creation-annihilation of a vortex pair can be understood in terms of the real and imaginary loci crossing and uncrossing.

B. Fixed tuning with phase evolution

Figure 7 shows interferograms and zero loci of the field under the condition that the resonator length is approximately constant. In this case, the amplitudes, $C_0/C_1/C_4$, of the constituent modes are effectively constant while the relative phase differences continue to evolve. It can be seen from the interferogram in Fig. 7(a)(i) there is once again a fifth dark region without a dislocation in the field. The real and imaginary zero loci, Fig. 7(b)(i), do not intersect but are almost tangential. When the phase has evolved by an amount, Fig. 7(a)(ii), the dark region now has a vortex of the same charge as the other vortices and a second vortex is also created, which is roughly central with opposite charge. The boxed vortex in Fig. 7(a)(ii) corresponds to the indicated innermost intersection of real and imaginary zero loci in Fig. 7(b)(ii). Further evolution of the phase shows that the central vortex is no longer present and one of the outer vortices is now annihilated with only the dark region indicated being present. In this manner, a vortex pair is created, one vortex of which remains on the circle trajectory and the other moves inward. The inner vortex moves around and then annihilates with one of the other outer vortices so that for a fixed resonator tuning, a vortex pair is created and annihilated periodically, as the phase evolves.

V. FREQUENCY NONDEGENERACY OF HELICAL MODES IN A NONPLANAR RING RESONATOR

The observed circling vortex patterns have been described using a superposition of passive cavity modes, A_0, A_1^-, and

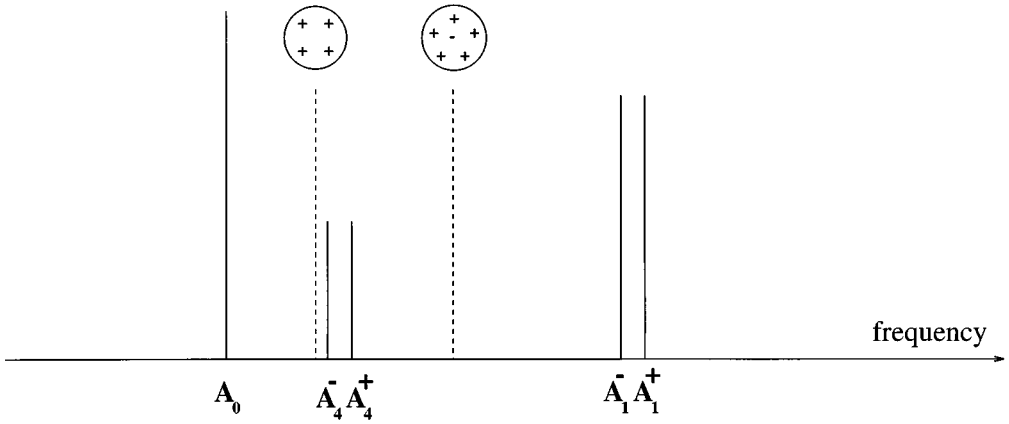

FIG. 8. Relationship between cavity modes and circling vortex patterns as in Fig. 3 but assuming frequency nondegenerate doughnut modes. The situation depicted is consistent with the observed number, distribution, and charge of vortices observed in the patterns investigated.

A_4^+. Since each of these is from different transverse mode families ($q=0,1,4$, respectively) the corresponding cavity frequencies are different. However, the opposite topologically charged modes A_1^+ and A_4^- are frequency degenerate with A_1^- and A_4^+, respectively, the only difference being the sense of change of the phase about the optic axis with distance along this axis. Thus the following combinations of modes ought to be equally well observable:

$$A_0+A_4^+; \quad A_0+A_4^-, \qquad (7)$$

$$A_1^-+A_4^+; \quad A_1^+ + A_4^-; \quad A_1^+ + A_4^+; \quad A_1^- + A_4^-.$$

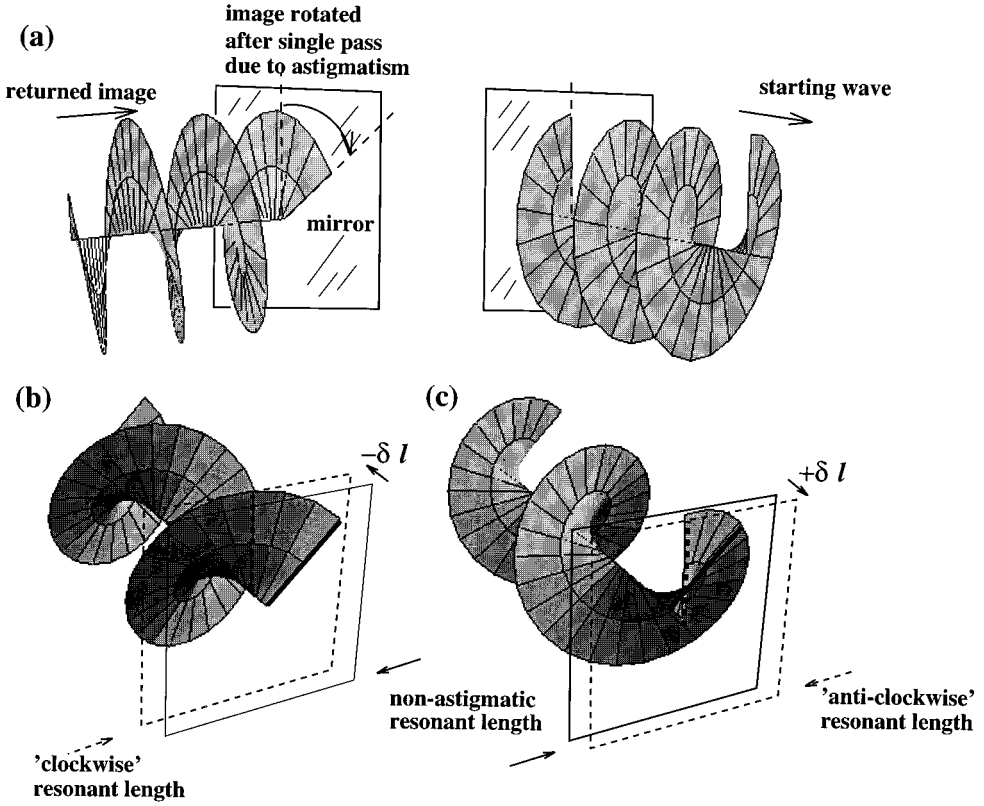

FIG. 9. (a) Schematic representation of the effect of astigmatic cavity image rotation upon a helical mode, which is otherwise resonant with the cavity. The image rotation corresponds to a phase shift causing the phase of the wave returning after a single pass to no longer be the same as the starting phase. (b),(c) Frequency nondegeneracy of oppositely charged helical waves in such a cavity. The solid square plane represents the resonant length of the cavity without astigmatism. For the clockwise wave (b), the dotted plane is the position to which the cavity must be tuned so that the phase is the same after one round trip (dotted phase line). The anticlockwise wave (c) requires a lengthening of the cavity in order to be resonant.

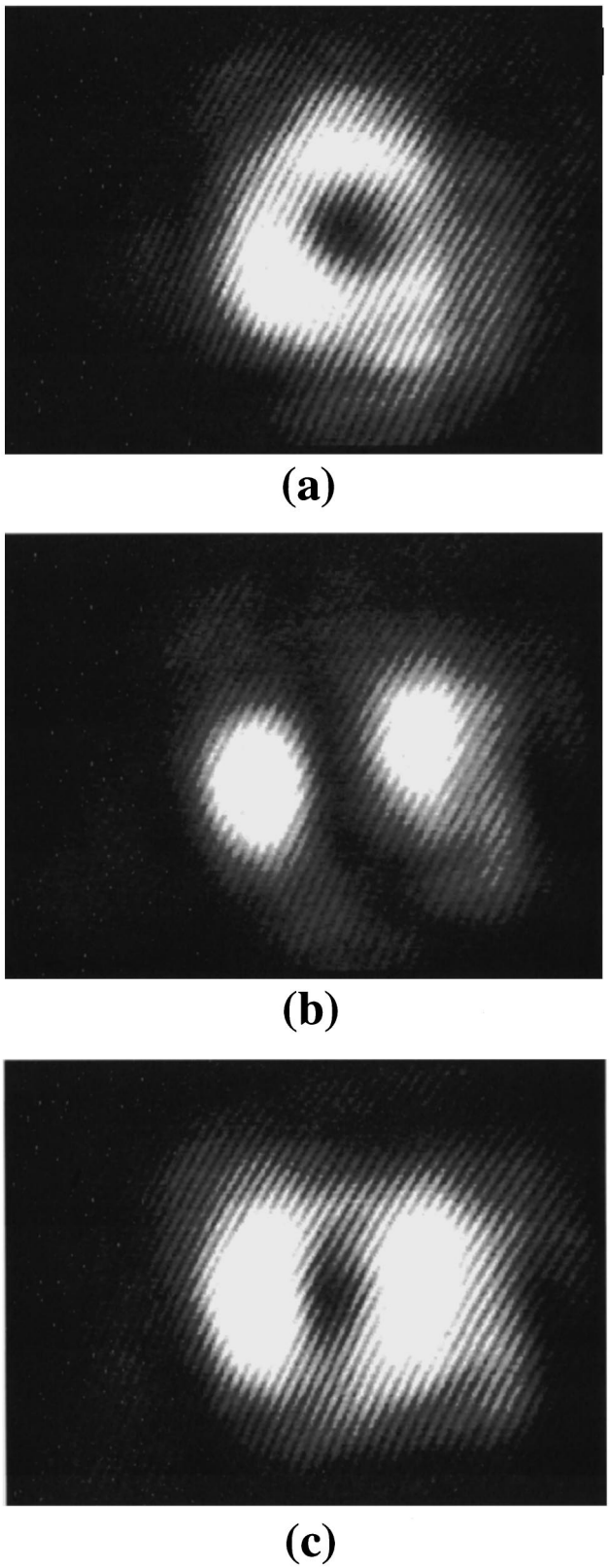

FIG. 10. Output patterns of the PRO for three tuning positions near the charge 1 doughnut mode using a significantly nonplanar cavity. (a) Doughnut mode with interference fringe ''fork'' point ''up.'' (b) TEM_{01} mode, which is the superposition of a plus 1 and minus 1 doughnut mode. (c) Doughnut mode with interference fringe ''fork'' point ''down.''

The first two superpositions listed above both result in 4 circling vortices. The 4 vortices all have identical topological charge in one superposition and the opposite for the other superposition. Thus the difference in the observed pattern would only be apparent in the interferograms. The superpositions of $A_1^- + A_4^+$ and $A_1^+ + A_4^-$ again differ only by a reversal of topological sign of all vortices between patterns. The number and distribution of vortices are the same in both superpositions. The reversal of vortex charge was not observed in any of the interferograms for switches between circling vortex patterns. Furthermore, the superpositions $A_1^+ + A_4^+$ and $A_1^- + A_4^-$ have 3 vortices circling a central fourth vortex. These patterns were also never observed, indicating that the superposition of the same helical modes, $A_1^- + A_4^+$, was always observed.

This can be explained if oppositely charged helical modes are frequency nondegenerate (we will demonstrate this below). In this case, Fig. 3 is then more accurately replaced by Fig. 8 where, to avoid clutter, just the center frequencies of the now nondegenerate resonances are shown by vertical lines. Oppositely charged doughnut modes A_1^- and A_1^+ and also A_4^- and $^+_4$ are represented as having different frequencies. Given the arrangement of Fig. 8, it can be seen that for the tuning position between the $q=4$ and $q=1$ mode families, only the $A_1^- + A_4^+$ superposition is expected. It may be argued that when tuning is changed to between the $q=1$ and $q=0$ modes, the superposition should involve the A_4^- rather than the A_4^+ helical mode. If this were so, then as the tuning is changed between positions, the sign of the outer circling vortices should reverse. This is not observed, as shown in Fig. 2. The reason is that there is a certain amount of hysteresis between competing modes [1,7] so that once the pattern based on A_4^+ is set up, it persists with further tuning.

Such a frequency difference between oppositely charged helical modes of the same charge strength can be explained by image rotation in the cavity. The effect is illustrated in Fig. 9 using a charge 1 helical mode. As mentioned earlier, rotation of a helical mode corresponds to a phase shift. If the cavity is resonant for a particular mode then after one round trip, the phase of the field returns to the starting value and the mode is supported by the cavity. By introducing ''astigmatism'' such that an image is rotated after one round trip, Fig. 9(a), the phase of a helical field will no longer be the same as the starting value. In the figure, the phase of the helical mode has advanced too far. However, if the cavity length is shortened, it can be ''tuned'' to the length where the phase is the same as the starting value, as illustrated in Fig. 9(b). Figure 9(c) shows that for an oppositely charged mode, the cavity length has to be lengthened to allow the phase to return to the starting value after a round trip. Thus for the sense of image rotation given in the figures, the ''clockwise'' mode has a higher frequency than the anticlockwise mode. This situation is reversed if the sense of rotation of the image with propagation of the optical mode is opposite to that depicted.

The physical mechanism of image rotation is due to a nonplanar arrangement of the optic axis of the cavity [8]. A misplacement of the beam height of 0.5 mm on one mirror, for example, yields a 0.6° image rotation. Equating the percentage image rotation to a percentage phase change for two oppositely charged helical modes gives a frequency differ-

ence (compared to that of the nonrotated, frequency degenerate modes in a planar cavity) of $\pm 0.15\%$ of a free spectral range (f.s.r.) and hence a separation of 0.3% f.s.r. between oppositely charged modes. This is significant enough to create the situation depicted in Fig. 8.

To exaggerate the effect of a nonplanar cavity, the experimental system was realigned so as to deliberately misplace the beam height at one of the ring cavity mirrors by approximately 5 mm. This translates to a frequency separation between oppositely charged doughnut modes of 3.2% f.s.r., which is large enough to allow a piezo controlled tuning through the nondegenerate modes. Figure 10 shows the interferograms of observed patterns when tuning near a charge 1 doughnut mode using a nonplanar cavity. For the change in frequency tuning between (a) and (c), the change in sign of the topological charge of the doughnut mode is apparent. Figure 10(b) is the superposition of the two oppositely charged modes, which, interestingly, appear not to compete here. In general this superposition rotates as the two constituent modes are emitted at different frequencies. We have reported such a rotation in [5].

VI. CONCLUSION

We have shown an experimental instance where a smooth metamorphosis between two different transverse patterns of a PRO occurs through the creation or annihilation of an optical-vortex pair. The pair is created for a transition between circling vortex patterns where the number of vortices between patterns changes by two and the total topological charge between these patterns remains the same. The vortex-pair creation and subsequent annihilation has been shown for a stroboscopically sampled angular position of the location of pair creation as the resonator is tuned. Also shown is pair creation for a fixed resonator tuning for which the phase of the optical field continues to evolve. The number of vortices, their arrangement, topological charge, circling direction, and transition dynamics can be well represented by a linear superposition of empty cavity helical modes with variable phases between the mode fields thus validating the assumption that the observed modes are in quasiequilibrium with the particular tuning position of the cavity. The creation (annihilation) of the vortex pair is observed in the superposition calculation showing the intersections of the zeros of the real and imaginary parts of the field.

We have also demonstrated that otherwise frequency degenerate helical modes of the same charge magnitude but opposite sign become nondegenerate when an image-rotation astigmatism is introduced into the optical resonator (as a consequence on a nonplanar cavity). This is the reason that the observed patterns are always composed of helical modes of one particular topological charge when the oppositely charged modes are equally well expected. The effect of frequency splitting of these helical modes was deliberately exaggerated and experimentally measured for the charge 1 doughnut mode.

ACKNOWLEDGMENTS

Part of this work is supported by funds from Fr.-Naumann Stiftung and the Leibnitz Program of the Deutsche Forschungsgemeinschaft.

[1] M. Vaupel and C. O. Weiss, Phys. Rev. A **51**, 4078 (1995).
[2] D. Hennequin, L. Dambly, D. Dangoisse, and P. Glorieux, J. Opt. Soc. Am B **11**, 676 (1994).
[3] A. Yariv and S. K. Kwong, Opt. Lett. **10**, 454 (1985).
[4] P. Yeh, J. Opt. Soc. Am. B **2**, 1924 (1985).
[5] J. Malos, M. Vaupel, K. Staliunas, and C. O. Weiss, Phys. Rev. **53**, 3559 (1996).
[6] P. Coullet, L. Gil, and F. Rocca, Opt. Commun. **73**, 403 (1989).
[7] K. Staliunas, M. F. H. Tarroja, G. Slekys, C. O. Weiss, and L. Dambly, Phys. Rev. A **51**, 4140 (1995).
[8] D. Berkowitz, J. Opt. Soc. Am. **55**, 1464 (1965).